Finite-difference calculation of the Green's function of a one-dimensional crystal: Application to the Krönig-Penney potential

A. Mayer*

Laboratoire de Physique du Solide, Facultés Universitaires Notre-Dame de la Paix, Rue de Bruxelles 61, B-5000 Namur, Belgium

(Received 14 February 2006; revised manuscript received 29 June 2006; published 24 October 2006)

We present a finite-difference scheme for computing the Green's function of a one-dimensional crystal. The method enables one to derive the band structure and the density of states of this type of structures, whatever the particular values of the potential energy. The technique also enables one to compute the influence of defects on the density of states and on the scattering of the eigenstates of the crystal. The technique is applied to the Krönig-Penney potential. In particular, we study the bound states of a square potential introduced in the crystal and their influence on the conductance of the system. We also determine the surface states induced by a termination of the Krönig-Penney potential. Our results turn out to be in excellent agreement with analytical expressions, which proves their validity and the versatility of the technique.

DOI: 10.1103/PhysRevE.74.046708 PACS number(s): 02.70.Bf, 71.15.−m, 71.20.−b, 73.20.At

I. INTRODUCTION

Green's functions [1–10] and finite-difference techniques [11–14] have proven to be efficient tools in the modeling of many problems in physics. These techniques can indeed be adapted to a wide range of situations for which analytical solutions do not exist. The domains to which these methods apply include quantum mechanics [1–6], acoustics [7], electromagnetism [8–14], etc. In addition to this wide applicability, these two techniques have the advantage to be stable and numerical schemes that still improve their efficiency are frequently presented [5,6,10,13,14].

Green's functions are usually applied to the study of local perturbations such as defects [10], interfaces [3,9], or point excitations in a system [8]. They also give access to intrinsic properties of these systems, like the local density of states or conduction properties. In order to apply this technique, one has to determine the Green's function of the unperturbed problem (without the defect), which usually requires some preliminary analytical or computational effort. Finite-difference techniques, on the other hand, replace derivatives by their numerical counterpart, so that differential equations are eventually turned into a set of linear equations [11–14]. Their resolution is then achieved, in the simplest form of the algorithm, using standard linear-algebra routines. The strength of this method consists in its applicability to a wide range of equations, regardless of the particular functions that enter these equations.

The combination of these two techniques leads to the "discrete Green's function" method [15,16]. In this approach the Green's-function methodology is actually considered as a means to solve finite-difference equations. Reversing the point of view, we consider in this paper the finite-difference technique as a means to determine the Green's function of periodic one-dimensional systems. This gives an easy access to intrinsic properties of these systems as well as to the influence of defects.

The paper starts in Sec. II with the development of a finite-difference construction of the Green's function of a periodic one-dimensional system. We also present extensions for studying the influence of defects on the density of states (Sec. III) and the scattering of the eigenstates of the crystal (Sec. IV). Due to its pedagogical value in condensed matter physics and the availability of analytical results, we apply in Sec V this methodology to the Krönig-Penney potential [17,18]. In particular, we compute the band structure and the density of states associated with this potential. We also study the influence of a potential well on the density of states and the conductance of the crystal. Finally, we determine the surface states of the Krönig-Penney potential. Our results turn out to be in excellent agreement with analytical expressions, which proves their validity and the versatility of the technique.

II. FINITE-DIFFERENCE CALCULATION OF THE GREEN'S FUNCTION OF A ONE-DIMENSIONAL CRYSTAL

A. Supercell representation of the one-dimensional crystal

We describe the one-dimensional crystal as the periodic repetition of a supercell made of M elementary cells, which describe either the basic unit of the perfect crystal or a defect in that crystal. Each elementary cell is discretized along N points separated by a distance Δx ($\Delta x = L/N$, where L is the length of the elementary cells). Each position in the crystal is therefore defined by the subscripts (i,j), where $j \in [1,M]$ refers to the elementary cells of the crystal and $i \in [1,N]$ refers to the discretization steps within each cell. The position x that corresponds to the subscripts (i,j) is therefore given by $x = i\Delta x + (j-1)L$. Within this representation of the crystal, the first Brillouin zone is discretized along the wave vectors $k = -\frac{\pi}{L} + \left(l - \frac{1}{2}\right)\frac{2\pi}{ML}$, where $l \in [1,M]$.

This sampling of the Brillouin zone with increments of $\frac{2\pi}{ML}$ is the consequence of our assumption that the crystal is the periodic repetition of supercells made of M elementary cells. This assumption gives therefore the physical context of this sampling and enables one to control the consequences of this sampling: essentially the overlapping of solutions whose extension would be larger than the length of the supercell.

*Electronic address: alexandre.mayer@fundp.ac.be

These overlapping effects are easily controlled by taking M sufficiently large. For the calculation of the band structure presented in Sec. II B, any other sampling of the Brillouin zone could actually be chosen. For the determination of the Green's function developed in Sec. II C, Bloch's theorem, however, requires that only wave vectors separated by increments of $\frac{2\pi}{ML}$ be selected. Considering another type of sampling may be numerically efficient, but would miss the physical grounds given here. The $\frac{1}{2}$ that appears in the definition of k is arbitrary and prevents this quantity from being zero. When $k=0$, it is indeed not possible to distinguish between states propagating to the left of the system from states propagating to the right, and this leads to numerical difficulties when computing the scattering of the eigenstates of the crystal as in Sec. IV.

B. Calculation of the eigenstates of the crystal

Applying finite-difference techniques, one can discretize Schrödinger's equation in the form

$$-\frac{\hbar^2}{2m}\frac{\psi_{i-1}-2\psi_i+\psi_{i+1}}{\Delta x^2}+V_i^0\psi_i=E\psi_i, \tag{1}$$

where ψ_i and V_i^0 refer to the wave-function and potential-energy values at $x=i\Delta x$ in the perfect crystal (i.e., with no defect). The particular value of the cell number j is not important at this point as the elementary cells of the perfect crystal are all identical. The accuracy of our algorithm may actually be improved by using the Numerov approximation of the second derivative [19,20], but this idea will not be developed in the current paper.

In order to compute the Bloch states of the crystal, we pose as boundary conditions $\psi_0=\psi_N\exp(-ikL)$ and $\psi_{N+1}=\psi_1\exp(ikL)$, where the wave vector k is chosen in the first Brillouin zone according to the prescription given in the previous section. We can then solve for $\{\psi_1,\psi_2,\ldots,\psi_N\}$. This leads to the eigenvalue equation

$$\begin{pmatrix} d_1 & s & & & se^{-ikL} \\ s & d_2 & s & & \\ & \ddots & \ddots & \ddots & \\ & & s & d_{N-1} & s \\ se^{ikL} & & & s & d_N \end{pmatrix}\begin{pmatrix}\psi_1\\ \psi_2\\ \vdots\\ \psi_{N-1}\\ \psi_N\end{pmatrix}=E\begin{pmatrix}\psi_1\\ \psi_2\\ \vdots\\ \psi_{N-1}\\ \psi_N\end{pmatrix}, \tag{2}$$

where $d_i=\frac{\hbar^2}{2m}\frac{2}{\Delta x^2}+V_i^0$ and $s=-\frac{\hbar^2}{2m}\frac{1}{\Delta x^2}$.

The eigenvalues $E^{n,k}$ of this system provide the energies relevant to the band structure of the crystal. The superscript n enumerates energies associated with a given value of k. In the remaining parts of this paper, we restrict the set of solutions to those that satisfy $E^{n,k}\leqslant E_{\text{cutoff}}$ and it is only necessary to be able to enumerate those solutions (the particular value of n is of no fundamental importance).

We will refer by $\psi_i^{n,k}$ to the components of the eigenvector associated with $E^{n,k}$. We assume them to be orthonormalized according to $\Sigma_{i=1}^N(\psi_i^{n,k})^*\psi_i^{n',k}=\delta_{n,n'}$, where the symbol $*$ stands for the complex conjugate. The eigenstates of the crystal are then given by

$$\Psi_{i,j}^{n,k}=\frac{1}{\sqrt{M}}e^{ijkL}\psi_i^{n,k}, \tag{3}$$

where $|\Psi_{i,j}^{n,k}|^2$ must be interpreted as the probability that an electron in the state $\Psi^{n,k}$ (band n associated with a wave vector k) is situated in the step i of the cell j. These quantities $\Psi_{i,j}^{n,k}$ are actually related to the physical wave function $\Psi_{\text{phys}}^{n,k}$ by the relation $\Psi_{\text{phys}}^{n,k}[i\Delta x+(j-1)L]=\frac{\Psi_{i,j}^{n,k}}{\sqrt{\Delta x}}$.

This definition of the eigenstates of the crystal is consistent with Bloch's theorem as $\Psi_{\text{phys}}^{n,k}(x+L)=e^{ikL}\Psi_{\text{phys}}^{n,k}(x)$. These states turn out to be normalized on the supercell of the crystal ($\Sigma_{j=1}^M\Sigma_{i=1}^N|\Psi_{i,j}^{n,k}|^2=1$). One can also check that they are orthonormal to each other, in the sense that $\Sigma_{j=1}^M\Sigma_{i=1}^N(\Psi_{i,j}^{n,k})^*\Psi_{i,j}^{n',k'}=\delta_{n,n'}\delta(k-k')$, and that the set is complete. These states thus form an appropriate basis for the following parts of this development.

C. Derivation of the Green's function of the crystal

Using the spectral decomposition of the Green's function, one can derive its components in our supercell representation of the crystal. These components turn out to be given by

$$G_{i,j;i',j'}^0(z)=\sum_{n,k}\frac{\Psi_{i,j}^{n,k}(\Psi_{i',j'}^{n,k})^*}{z-E^{n,k}}=\frac{1}{M}\sum_{n,k}\frac{e^{i(j-j')kL}\psi_i^{n,k}(\psi_{i'}^{n,k})^*}{z-E^{n,k}}, \tag{4}$$

where $z=E+i0^+$ contains the electron energy E and a small positive imaginary component $i0^+$ associated with the lifetime $\tau=\hbar/0^+$ of the states being considered. This expression is used for the calculation of the density of states (see Sec. III).

Mathematically and because of the physical interpretation of $i0^+$, this quantity also determines the width of the contribution of each state $\Psi^{n,k}$ to the density of states (see Sec. III). Ideally, for the study of stationary states, 0^+ should be taken to the limit $0^+\to 0$. In practice, 0^+ is made as small as possible to reduce its impact on computed results. It must, however, keep a value sufficiently large to compensate for the finite number of states $\Psi^{n,k}$ actually considered for the calculation of the density of states (discontinuous results are indeed obtained when 0^+ is too small). 0^+ is typically of the order of the energy separation between adjacent points in the band structure, this quantity being inversely proportional to M. In the applications presented in this paper, we took $N=80$, $M=8000$, and $0^+=0.002$ eV, which provides results with a typical accuracy of 0.001 eV. As stated previously, the summation in Eq. (4) is restricted to the states that satisfy $E^{n,k}\leqslant E_{\text{cutoff}}$. In order to reach an accuracy of 0.001 eV in the applications presented hereafter, we took $E_{\text{cutoff}}=30$ eV (which is 20 eV larger than the highest energy considered for the calculation of the density of states or that of the transmission coefficient). The sensitivity of the results of this paper to the particular values of N, M, 0^+, and E_{cutoff} is given with more details in Appendix A.

When calculating the scattering of the eigenstates of the crystal (see Sec. IV), the energy E is one of the $E^{n,k}$. In situations where the potential energy is real valued and as-

suming that $\Psi^{n,k}$ is a right-going solution, the components of the Green's function can be computed more efficiently using the expression

$$G^0_{i,j;i',j'}(E^{n,k}) = \frac{4m\Delta x^2}{\hbar^2}\begin{cases} \dfrac{(\Psi^{n,k}_{i,j})^*\Psi^{n,k}_{i',j'}}{W} & \text{when } \mathrm{pos}(i,j) \leqslant \mathrm{pos}(i',j'), \\ \dfrac{(\Psi^{n,k}_{i',j'})^*\Psi^{n,k}_{i,j}}{W} & \text{when } \mathrm{pos}(i,j) > \mathrm{pos}(i',j'), \end{cases} \tag{5}$$

where $\mathrm{pos}(i,j)=i\Delta x+(j-1)L$ and $W=(\Psi^{n,k}_{i,j})^*[\Psi^{n,k}_{i+1,j}-\Psi^{n,k}_{i-1,j}] - \Psi^{n,k}_{i,j}[(\Psi^{n,k}_{i+1,j})^*-(\Psi^{n,k}_{i-1,j})^*]$ is the numerical equivalent of the Wronskien [9]. This quantity turns out to be constant in the crystal, so that the particular values of i and j where this quantity is evaluated is of a reduced significance (in order to be as accurate as possible, W is actually evaluated by taking its average on the N points of an elementary cell). The derivation of Eq. (5) as well as the degree of variability of W is given in more detail in Appendix B.

III. CALCULATION OF THE DENSITY OF STATES OF THE CRYSTAL

The density of states of the perfect crystal can be calculated using the expression

$$n_0(E) = \sum_{n,k} \delta(E-E^{n,k}) = -\frac{1}{\pi}\,\mathrm{Im}\sum_{n,k}\frac{1}{z-E^{n,k}}, \tag{6}$$

where $z=E+i0^+$ ($0^+=0.002$ eV) [1]. The results obtained using the formal expression $n_0(E)=-\frac{1}{\pi}\,\mathrm{Im\,Tr}\,G^0(E+i0^+)$ are identical, but in practice this second method is less efficient because of the time required to compute the components of the Green's function.

The modification in the density of states that results from a defect introduced in the crystal can be calculated with this second expression

$$\Delta n(E) = -\frac{1}{\pi}\frac{d}{dE}\,\mathrm{Im\,ln\,det}(1_{AA}-\mathbf{G}^0_{AA}\mathbf{V}_{AA}), \tag{7}$$

where the subscript A refers to the region that supports the perturbation potential [1]. The matrices $\mathbf{1}_{AA}$, $\mathbf{G}^0_{AA}$, and $\mathbf{V}_{AA}$ contain the components of, respectively, the unit matrix, the Green's function $G^0(z)$, and the perturbation potential V in the region A. This formula involves a matrix multiplication between the matrices $\mathbf{G}^0_{AA}$ and $\mathbf{V}_{AA}$. For a defect that extends on the N points of the cell $j=M/2$ (like in Secs. IV A–IV D, the region A consists of the points $(1,M/2),(2,M/2),\ldots,(N,M/2)$ so that the dimension of the matrices $\mathbf{1}_{AA}$, $\mathbf{G}^0_{AA}$, and $\mathbf{V}_{AA}$ is N. The elements of the Green's function are calculated using Eq. (4).

IV. CALCULATION OF THE SCATTERING OF THE EIGENSTATES OF THE CRYSTAL

We focus here on the scattering of the eigenstates $\Psi^{n,k}$ of the crystal. In particular we only consider states that propagate initially to the right (i.e., states associated with a positive current density). The standard procedure [2] consists in solving first the equation

$$(\mathbf{1}_{AA}-\mathbf{G}^0_{AA}\mathbf{V}_{AA})\mathbf{\Psi}_A = \mathbf{\Psi}^0_A, \tag{8}$$

where $\mathbf{\Psi}^0_A$ is a vector that contains the components of the incident state $\Psi^{n,k}$ in the perturbation region A. The vector $\mathbf{\Psi}_A$ contains after resolution of this equation the values of the scattered wave function. This formula involves a matrix multiplication between the matrices $\mathbf{G}^0_{AA}$ and $\mathbf{V}_{AA}$, as well as between the matrix $(\mathbf{1}_{AA}-\mathbf{G}^0_{AA}\mathbf{V}_{AA})$ and the vector $\mathbf{\Psi}_A$. For a defect extending on the N points of the cell $j=M/2$, the dimension of the vectors $\mathbf{\Psi}^0_A$ and $\mathbf{\Psi}_A$ is N. The elements of the Green's function are calculated this time using Eq. (5).

In a second step, one can use the equation

$$\mathbf{\Psi}_B = \mathbf{\Psi}^0_B + \mathbf{G}^0_{BA}\mathbf{V}_{AA}\mathbf{\Psi}_A \tag{9}$$

to compute the scattered wave function in any region B of the crystal. The vectors $\mathbf{\Psi}^0_B$ and $\mathbf{\Psi}_B$ contain the components of, respectively, the incident state $\Psi^{n,k}$ and the scattered wave function in this region B. The matrix $\mathbf{G}^0_{BA}$ contains the components of the Green's function. This formula involves a matrix multiplication between the matrices $\mathbf{G}^0_{BA}$ and $\mathbf{V}_{AA}$ and the vector $\mathbf{\Psi}_A$. In order to compute the transmitted and reflected current densities, one actually needs the scattered wave function on two couples of adjacent points, situated immediately before and after the defect. For a defect extending on the N points of the cell $j=M/2$, the region B consists of the four points $(N-1,M/2-1)$, $(N,M/2-1)$, $(1,M/2+1)$, and $(2,M/2+1)$. The dimension of the vectors $\mathbf{\Psi}_B$ and $\mathbf{\Psi}^0_B$ is therefore 4, and $\mathbf{G}^0_{BA}$ is a $(4\times N)$ matrix.

For a real-valued potential energy, one can express the incident, reflected, and transmitted states as $\Psi^{n,k}$, $R\Psi^{n,k}$, and $T\Psi^{n,k}$, respectively. Combining Eqs. (5) and (9), the coefficients R and T turn out to be given by

$$R = \frac{4m\Delta x^2}{\hbar^2}\sum_{i,j\in A}\frac{\Psi^{n,k}_{i,j}V_{i,j}\Psi_{i,j}}{W}, \tag{10}$$

$$T = \frac{4m\Delta x^2}{\hbar^2}\sum_{i,j\in A}\frac{(\Psi^{n,k}_{i,j})^*V_{i,j}\Psi_{i,j}}{W}, \tag{11}$$

where $V_{i,j}$ refers to the values of the perturbation potential in the region A and $\Psi_{i,j}$ to the corresponding values of the scattered wave function [the $\Psi_{i,j}$ are just the components of the vector $\mathbf{\Psi}_A$ computed in Eq. (8)].

If (i,j) refers to points situated before the defect (region of incidence), the values of the incident and reflected parts of the wave function are, respectively, given by $\Psi^{\mathrm{in}}_{i,j}=\Psi^{n,k}_{i,j}$ and $\Psi^{\mathrm{refl}}_{i,j}=R(\Psi^{n,k}_{i,j})^*$. One can then compute the incident and reflected current densities by

$$J^{n,k}_{\mathrm{in}} = -\frac{\hbar}{m}\frac{|\Psi^{n,k}_{i+1,j}|^2}{\Delta x^2}\,\mathrm{Im}\,\frac{\Psi^{n,k}_{i,j}}{\Psi^{n,k}_{i+1,j}}, \tag{12}$$

$$J_{\text{refl}}^{n,k} = -\frac{\hbar}{m}\frac{|R(\Psi_{i+1,j}^{n,k})^*|^2}{\Delta x^2}\,\text{Im}\,\frac{(\Psi_{i,j}^{n,k})^*}{(\Psi_{i+1,j}^{n,k})^*}, \tag{13}$$

so that the reflection coefficient is finally given by $R = -J_{\text{refl}}^{n,k}/J_{\text{in}}^{n,k}$ [21]. For a defect extending on the N points of the cell $j=M/2$, these two expressions may be evaluated using $(i,j)=(N-1,M/2-1)$.

Similarly, if (i,j) refers to points situated after the defect (region of transmission), the values of the transmitted part of the wave function are given by $\Psi_{i,j}^{\text{out}} = T\Psi_{i,j}^{n,k}$. The transmitted current density is calculated by

$$J_{\text{out}}^{n,k} = -\frac{\hbar}{m}\frac{|T\Psi_{i+1,j}^{n,k}|^2}{\Delta x^2}\,\text{Im}\,\frac{\Psi_{i,j}^{n,k}}{\Psi_{i+1,j}^{n,k}}, \tag{14}$$

so that the transmission coefficient is finally given by $T = J_{\text{out}}^{n,k}/J_{\text{in}}^{n,k}$. For a defect extending on the N points of the cell $j=M/2$, this expression may be evaluated using $(i,j)=(1,M/2+1)$.

This transmission coefficient turns out to be related to the conductance at the energy $E^{n,k}$ by $G=\frac{2e^2}{h}T$ (the regions of incidence and transmission are indeed identical and there is a single incident and transmitted state for a given value of the energy). Considering the contribution of each energy level $E^{n,k}$ and taking account of their occupancy (as described by the Fermi-Dirac distribution $f(E)=1/\{1+\exp[\beta(E-E_F)]\}$, in which $\beta=1/k_BT$, T is the temperature, and E_F is the Fermi level), one can demonstrate that the conductance at zero bias of the whole system is given by

$$G = \left.\frac{dI}{dV}\right|_{V=0} = 2e^2\sum_{n,k} J_{\text{out}}^{n,k}\frac{\beta\exp[\beta(E^{n,k}-E_F)]}{\{1+\exp[\beta(E^{n,k}-E_F)]\}^2}$$
$$\overset{T\to 0}{=} 2e^2\sum_{n,k} J_{\text{out}}^{n,k}\delta(E^{n,k}-E_F). \tag{15}$$

The results obtained using this relation turn out to be consistent with those obtained from the transmission coefficient.

V. APPLICATION TO THE KRÖNIG-PENNEY POTENTIAL

Due to its pedagogical value in condensed matter physics and because of the availability of analytical results, we will apply the technique developed in the previous sections to the Krönig-Penney potential [17,18]. The perturbation will consist of a square potential well [22–25]. Our study will also include the surface properties of the crystal. Previous work has essentially described this surface by a step potential [26–32]. The present article, which also includes the image potential, opens therefore interesting perspectives.

The length L of the elementary cells will be 0.5 nm. As mentioned previously, we take $N=80$ discretization steps in each cell, $M=8000$ cells for the periodic unit of the crystal, $0^+=0.002$ eV, and a cutoff energy E_{cutoff} of 30 eV. This enables one to get a typical accuracy of 0.001 eV in the applications presented hereafter. For applications where a resolution of 0.01 eV is sufficient, it is appropriate to take $N=40$, $M=2000$, $0^+=0.006$ eV, and $E_{\text{cutoff}}=20$ eV. The influence of these parameters on the accuracy of our results is given in more detail in Appendix A.

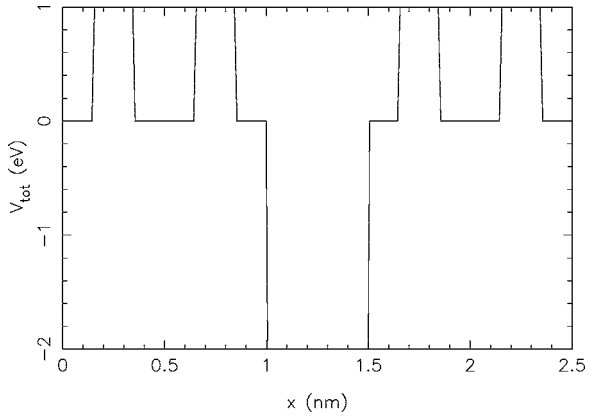

FIG. 1. Potential energy in the Krönig-Penney crystal. The perturbation consists of a square 2-eV potential well. Each cell is discretized with $N=80$ steps. The representation includes two elementary cells of the perfect crystal on each side of the perturbation ($M=8000$ cells are considered in the simulations).

The potential V^0 in the perfect crystal consists of square barriers with a width W of 0.2 nm and a height U of 1 eV, which are placed symmetrically in the middle of each cell. The perturbation V we consider first extends on a single cell ($L=0.5$ nm) and changes the potential V^0 of that cell into $V_{\text{tot}}=V^0+V$, which is a 2-eV potential well. The perturbation V is therefore given by $V=V_{\text{tot}}-V^0$, where V_{tot} is the total potential in the perturbation cell and V^0 the Krönig-Penney potential of the perfect crystal. The values of V_{tot} in the vicinity of the perturbation cell are represented in Fig. 1.

A. Band structure and density of states of the empty lattice

In order to enable a comparison with analytical results and highlight the influence of the Krönig-Penney potential, we first consider the case where the height U of this potential is zero (empty lattice). The problem is therefore reduced to that of an isolated square potential well.

As depicted in Fig. 2, the band structure of the perfect crystal is reduced to that of a periodic empty lattice. The representation includes results obtained using a plane-wave expansion of the wave function, which shows that excellent agreement with the finite-difference technique is achieved. The dependence of this agreement on the number of points, N, used to describe the elementary cell of the crystal is given in Appendix A. In Fig. 3, we represent the density of states $n_0(E)$ of the empty lattice (unperturbed potential) as well as the variation $\Delta n(E)$ in the density of states that results from the square potential.

The density of states $n_0(E)$ is actually calculated by three methods: (i) that given in Eq. (6), (ii) from the trace of the Green's function, and (iii) by the analytical expression $n_0(E)=\frac{2m}{h}\frac{ML}{\sqrt{2mE}}$ [$n_0(E)$ is the number of electronic states in the supercell of the crystal par unit energy] [18]. The three results are actually undistinguishable, which proves the validity of the technique. The way the accuracy of $n_0(E)$ actually

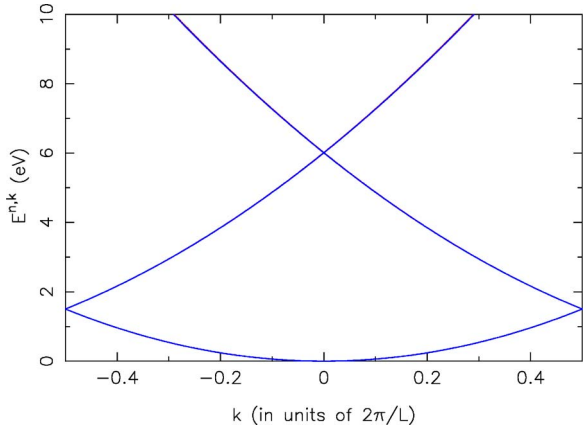

FIG. 2. (Color online) Band structure of the empty lattice, as obtained with the finite-difference technique and with a plane-wave representation of the wave function. The two results are undistinguishable.

depends on the parameters N, M, 0^+, and E_{cutoff} is also given in Appendix A.

The variation $\Delta n(E)$ of the density of states exhibits a negative peak at the opening of the first band, which reflects a reduction in the number of states proper to the empty lattice (because of the replacement of one cell of this lattice by the defect). The first positive peak, situated at −1.400 eV, is associated with the fundamental (symmetric) bound state of the square potential well. The second peak, situated at −0.081 eV, is due to the second (antisymmetric) bound state. The position of these two peaks is in close agreement with the values of −1.4007 eV and −0.0815 eV predicted by analytical models. It was checked that the transmission coefficient, as calculated using the techniques of Sec. IV, is also in close agreement with analytical results. The dependence of this agreement on the parameters of our model is given in detail in Appendix A.

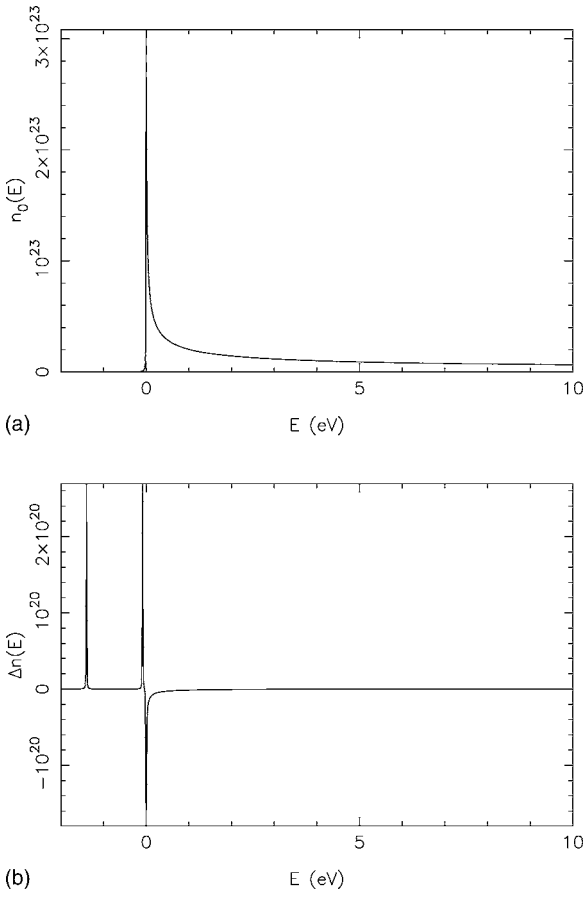

FIG. 3. Density of states $n_0(E)$ of the empty lattice (a) and variation $\Delta n(E)$ of the density of states due to the square potential well (b). $n_0(E)$ is calculated by three different methods (see text), but results are undistinguishable.

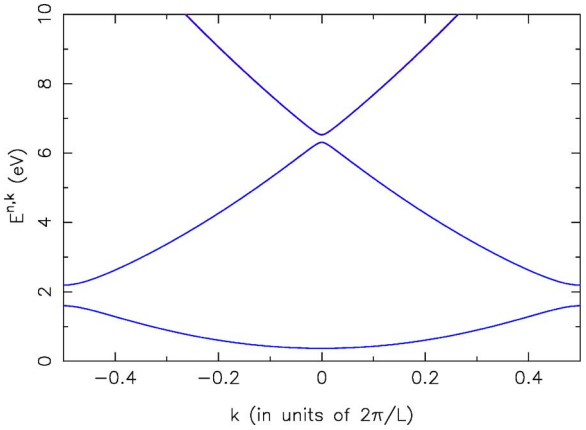

FIG. 4. (Color online) Band structure of the Krönig-Penney potential, as obtained with the finite-difference technique and with a plane-wave representation of the wave function. The two results are undistinguishable.

In the following sections of this paper, we will focus on the position of the first bound state of the potential well. This bound state extends indeed in the crystal as an evanescent state, with a decay length of 0.165 nm. This state therefore experiences the potential of the crystal, and its energy position must be influenced by the parameters of this potential.

B. Band structure, density of states, and scattering of the eigenstates of the Krönig-Penney potential

Setting $U=1$ eV, we consider now the Krönig-Penney potential as defining the elementary cell of the perfect crystal. The band structure corresponding to this new situation is represented in Fig. 4. The figure includes results obtained with a plane-wave expansion of the wave function, which proves again excellent agreement with the finite-difference formalism (this agreement is described more quantitatively in Appendix A). Compared to the empty lattice, the bands are uplifted approximately by $\frac{UW}{L}$ (which gives 0.40 eV, instead of 0.37 eV in the simulation). The middle of the first gap can be approximated by $\frac{UW}{L}+\frac{\hbar^2}{2m}\left(\frac{\pi}{L}\right)^2$ (which gives 1.90 eV instead of 1.89 eV). Finally, from the Fourier components of the potential energy, the width of the first gap is provided by $\frac{2\tilde{U}}{\pi}\sin(\pi W/L)$ (this gives 0.60 eV instead of 0.59 eV in the simulation).

We represented the density of states $n_0(E)$ as well as its variation $\Delta n(E)$ due to the square potential well in Fig. 5.

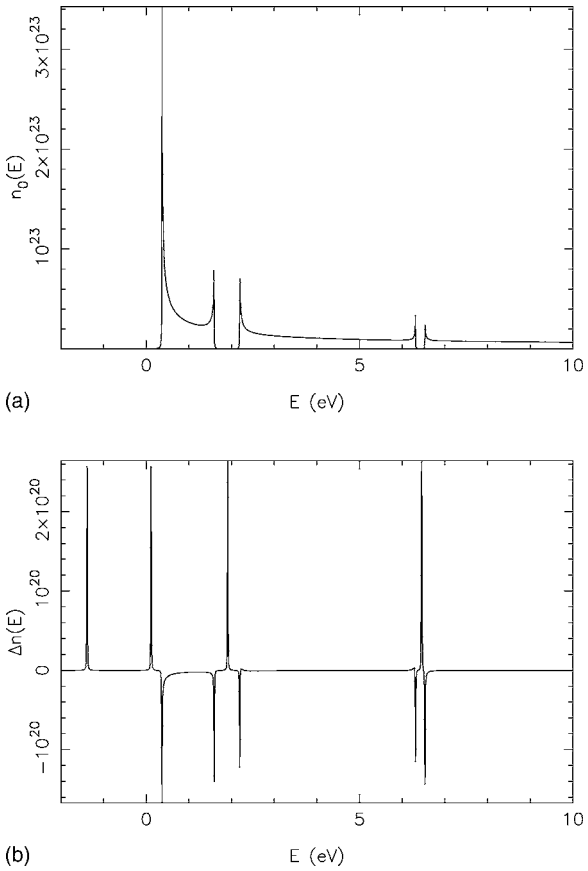

FIG. 5. Density of states $n_0(E)$ of the Krönig-Penney potential (a) and variation $\Delta n(E)$ of the density of states due to the square potential well (b).

The density of states $n_0(E)$ exhibits peaks at the opening or closing of the bands of energy (van Hove singularities). These singularities come from the fact $n_0(E)$ is inversely proportional to dE/dk, which cancels indeed at the opening or closing of the bands [33]. The density of states reflects of course the gaps observed in the band structure. The general aspect of this density of states is actually similar to that of a linear chain [34].

The variation $\Delta n(E)$ of the density of states exhibits negative peaks at the position of the van Hove singularities, which expresses again a reduction in the number of states proper to the crystal due to the replacement of one of its elementary cells by the defect. The first two positive peaks are the bound states already observed in the previous section. Their existence is bound to the evanescent nature of the wave function in the regions external to the defect (because the energy E of these states is below the first band of the crystal). The other peaks are of a similar nature. The evanescent character of these states (in the region external to the defect) is this time conditioned by the fact their energy E is in the band gap of the crystal. The position of the first two peaks is -1.39 eV and 0.12 eV. We will study in detail the dependence of the first peaks on the amplitude of the Krönig-Penney potential in the next section.

Figure 6 shows the transmission coefficient of the eigenstates of the Krönig-Penney potential. Without the square-potential perturbation, the transmission coefficient would take a unit value for each eigenstate of the crystal. The perturbation is responsible for a reduction of these values, especially in the vicinity of the opening or closing of bands of energy. Integrating this information in the way given in Eq. (15), one finally characterizes the whole system by its conductance G, which is $4.9\times10^{-6}\frac{2e^2}{h}$ (the Fermi level E_F was placed in the middle of the first gap like in most undoped semiconductors and a room temperature T of 300 K was assumed). We will study in a later section the dependence of the conductance on the depth of the square potential.

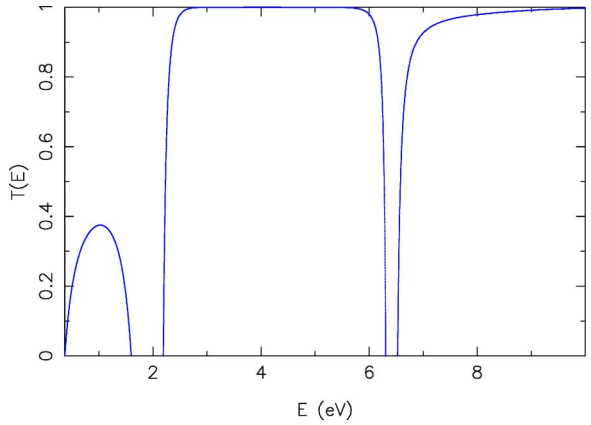

FIG. 6. (Color online) Transmission coefficient of the eigenstates of the Krönig-Penney potential. The perturbation consists of a square 2-eV potential well.

C. Dependence of the position of the first bound state of the square potential on the amplitude of the Krönig-Penney potential

We present in Fig. 7 the dependence of the first bound state of the square potential well on the amplitude U of the Krönig-Penney potential. When increasing U from 0 to 5 eV, we observe a monotonic increase of the peak position. This process is associated with the shortening of the decay length in the regions external to the defect. When U decreases from 0 to -5 eV, the peak position decreases

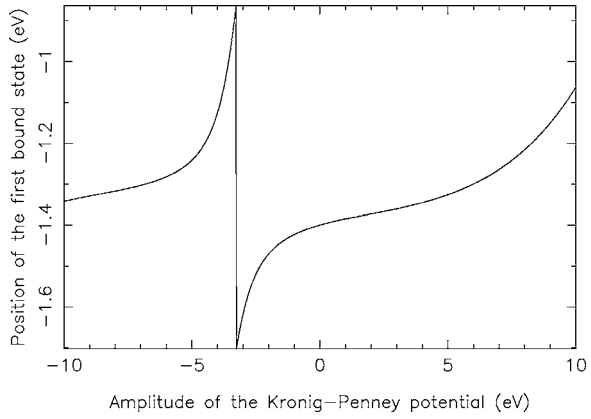

FIG. 7. Position of the first bound state of the square potential as a function of the amplitude of the Krönig-Penney potential.

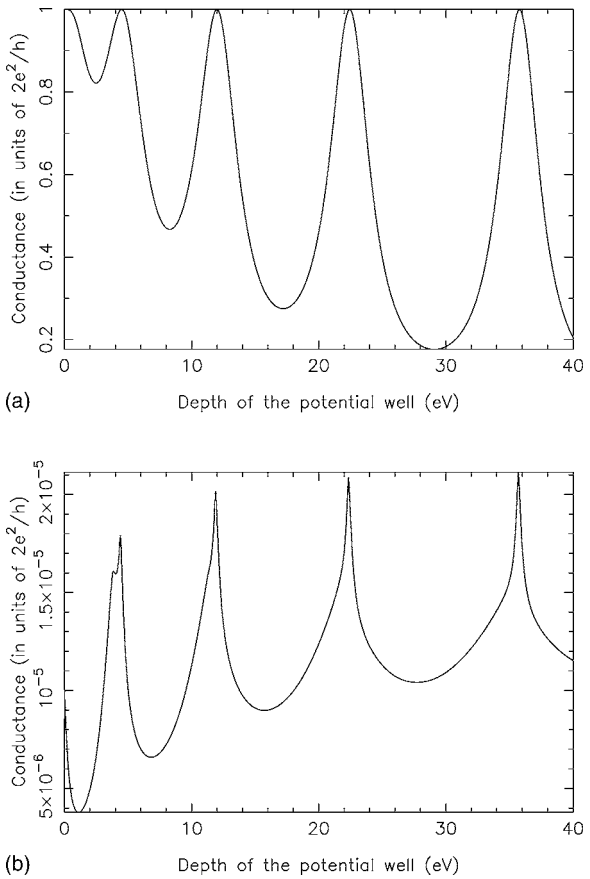

FIG. 8. Conductance of the system as a function of the depth of the square potential well. The amplitude U of the Krönig-Penney potential is 0 eV (a) and 1 eV (b).

monotonically except for a sharp transition at −3.26 eV. This transition occurs when the bottom of the first band finally crosses the energy level of the first bound state. The evanescent character of this bound state in the regions external to the defect becomes at this point associated with the fact the energy E of this state is in the band gap of the crystal (instead of being below the first band). The physical idea that regulates this sharp transition (displacement of the energy level by 0.84 eV for a variation of U smaller than 0.01 eV in our simulations) may find some practical interest in applications where the position of bound states is a sensitive parameter.

D. Dependence of the transmission of the eigenstates of the Krönig-Penney potential on the depth of the square potential well

We also studied the conductance of the system, as determined using Eq. (15) with a temperature T of 300 K and a Fermi energy placed in the middle of the first gap. In particular, we computed the dependence of the conductance on the depth of the square potential well. The results are illustrated in Fig. 8, where we considered the cases corresponding to $U=0$ (empty lattice) and $U=1$ eV (Krönig-Penney potential). The two results consist of a series of minima and maxima, which become increasingly separated as the depth

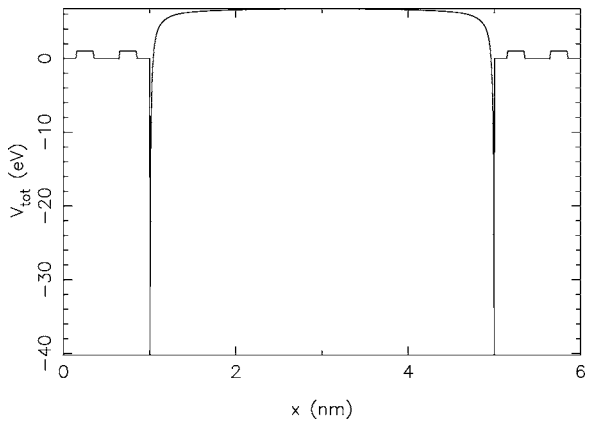

FIG. 9. Potential energy in the Krönig-Penney crystal. The perturbation extends on eight elementary cells of the crystal and consists of two surfaces described by an image potential. Each cell is discretized with $N=80$ steps. The representation includes two elementary cells of the perfect crystal on each side of the perturbation ($M=8000$ cells are considered in the simulations).

of the potential well increases. These maxima appear when there is a perfect match between the incident states (after propagation through the defect) and the outgoing states. This condition is essentially dependent on the behavior of the wave function in the defect, so that the maxima appear approximately at the same position in the two cases.

E. Surface states of the Krönig-Penney potential

We finally studied the surface states of the Krönig-Penney potential. Compared to previous work related to that topic [26–32], the current simulations are not restricted to the usual step-potential approximation and include the image interaction in the surface potential. The defect extends here on eight fundamental cells of the crystal and consists of two surfaces, which are represented by the image potential

$$V_{\text{image}}(d) = E_{\text{F}} + W - \frac{1}{4\pi\epsilon_0}\frac{\epsilon - 1}{\epsilon + 1}\frac{e^2}{4d}, \tag{16}$$

where d stands for the distance to either the left or right side of the defect (depending on which value is the smallest) [35]. We give the work function W a value of 5 eV and the relative permittivity ϵ a value of 10 (these values are typical for semiconducting materials). This situation is depicted in Fig. 9.

The variation $\Delta n(E)$ that results from this image potential is represented in Fig. 10. The negative peaks that appear at the opening or closing of bands of energy are associated with the reduction of states proper to the crystal, because of the replacement of eight fundamental cells by the defect. The peak at −0.17 eV is associated with a state that decays exponentially in the crystal, when leaving the defect. The existence of this state is permitted by the defect, as it prevents this exponential solution to grow unphysically in the opposite direction.

The two arrows indicate the energy position of the first bound states of the image potential, as obtained applying the

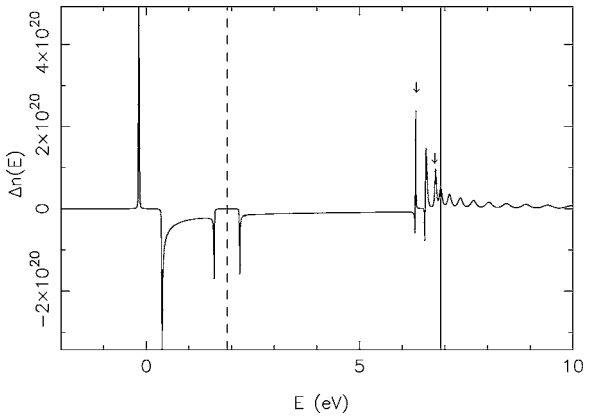

FIG. 10. Variation $\Delta n(E)$ of the density of states of the Krönig-Penney potential. The perturbation extends on eight elementary cells of the crystal and consists of two surfaces described by an image potential. The dashed and solid lines indicate, respectively, the Fermi level and the vacuum level. The arrows indicate the energy position of the first two bound states of the image potential, as obtained from an analytical formula that neglects the penetration of these states into the crystal.

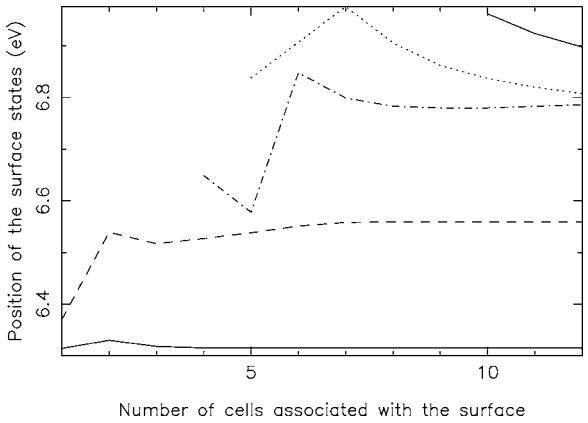

FIG. 11. Position of the surface states of the Krönig-Penney potential, as a function of the number of cells used to describe the surface. Each cell is represented with $N=80$ elementary steps and has a length of 0.5 nm. The results represent the first (solid line), the second (dashed line), the third (dot-dashed line), the fourth (dotted line), and the fifth (solid line, top right) surface states.

formula $E^n_{\text{image}}=E_F+W-\frac{13.60}{16n^2}\left(\frac{\epsilon-1}{\epsilon+1}\right)^2$ eV, where n enumerates the bound states [35,36]. This formula, which actually assumes that the bound states of the image potential do not penetrate into the crystal, gives an excellent account of the position of the first peak (which is in a band gap of the crystal). The other peaks are indeed associated with bound states of the image potential, but a substantial penetration into the Krönig-Penney crystal occurs. Their position is accurately accounted for by an independent model. Finally, the oscillations above the vacuum level are associated with standing waves in the defect. These oscillations become more contrasted and closer to each other as the length of the defect increases.

The extension of the defect considered in this simulation (eight fundamental cells) was sufficient to reproduce the energy position of the two first bound states with an accuracy of 1 meV (the error on the third peak is around 10 meV). In order to reproduce surface states associated with $n>3$, the surface region has to be given a larger extension. We represent in Fig. 11 the energy position of the first five surface states as a function of the number of fundamental cells used to represent the surface (each cell consists of $N=80$ elementary steps and has a length of 0.5 nm). The result shows that a minimum of four elementary cells is required in order to predict the position of the first bound state with an accuracy of 0.001 eV. The second bound state is obtained with the same accuracy using height elementary cells. The position of the third peak was calculated with up to 15 elementary cells. Considering the most accurate results, the three first surface states are finally found to be at an energy position of 6.315, 6.559, and 6.793 eV (−0.589, −0.345, and −0.111 eV relative to the vacuum level).

VI. CONCLUSION

We presented a finite-difference scheme for computing the Green's function of a one-dimensional crystal. The method enables one to derive the band structure and the density of states of this type of structures, whatever the particular values of the potential energy. The technique enables one to compute the influence of defects on the density of states on the transmission probability of the eigenstates of the crystal and on the conductance of the system.

As application of the technique, we investigated some properties of the Krönig-Penney potential. In particular, we studied how the energy level of the first bound state of a square potential well introduced in that crystal depends of the amplitude of the Krönig-Penney potential. We also studied how the conductance of the crystal is affected by the depth of the potential well. Finally, we computed the surface states of the Krönig-Penney potential. The comparison with analytical results confirm the validity of our results and prove the versatility of the technique.

ACKNOWLEDGMENTS

This work was supported by the National Fund for Scientific Research (FNRS) of Belgium. The author acknowledges the use of the Inter-university Scientific Computing Facility (ISCF) and the Belgian State Interuniversity Research Program on "Quantum size effects in nanostructured materials" (PAI/IUP P5/01). J.-P. Vigneron and C. Vandenbem are acknowledged for useful comments.

APPENDIX A: DEPENDENCE OF THE ACCURACY OF THE TECHNIQUE ON THE PARAMETERS N, M, 0^+, AND E_{cutoff}

This appendix presents with more details how the accuracy of our technique depends on the parameters N, M, 0^+, and E_{cutoff}. The band structure, as calculated using the technique of Sec. II B, is essentially affected by the parameter N. The parameter M indeed only determines the density of points in the band structure while E_{cutoff} merely specifies the upper limit to the energies being considered. From the com-

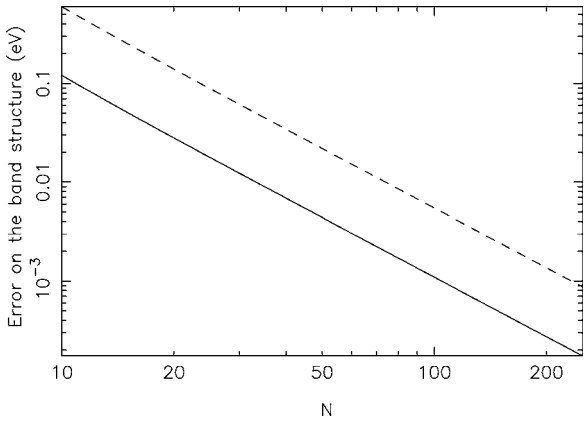

FIG. 12. Mean (solid) and maximal (dashed) error on the band structure presented in Fig. 2 (empty lattice), as a function of N. These errors are calculated for energies $E^{n,k} \leqslant 10$ eV.

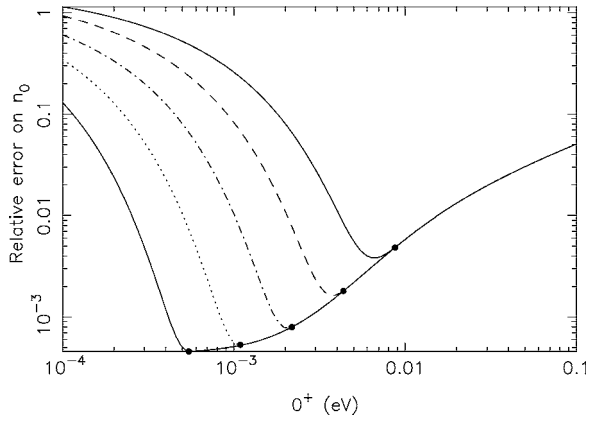

FIG. 13. Relative error on the density of states $n_0(E)$ of Fig. 3(a) (empty lattice), as a function of 0^+. These results are calculated using $N=80$, $E_{\text{cutoff}}=20$ eV, and $M=2000$, 4000, 8000, 16000, and 32000 (downwards). The points indicated the results obtained using 0^+_{opt} given by Eq. (A2) in the text.

parison with the results obtained using a plane-wave technique, it turns out that the error in the solutions corresponding to $E^{n,k} \leqslant E_{\text{cutoff}}$ is related to N and E_{cutoff} by a relation of the form

$$\epsilon_{\text{bands}} \sim E^2_{\text{cutoff}}/N^2. \tag{A1}$$

This relation provides the maximal error, which is actually achieved for $E^{n,k} \sim E_{\text{cutoff}}$ (the solutions with a lower energy are more accurate). We represent in Fig. 12 the average and maximal values of the error achieved on the results of Fig. 2 (band structure of the empty lattice). The results show that taking $N=74$ is sufficient to reach an accuracy always better than 0.01 eV (with an average accuracy of 0.002 eV considering the whole set of points represented in Fig. 2). In order to get an accuracy always better than 0.001 eV, it is necessary to take $N=234$.

The density of states $n_0(E)$, as calculated using Eq. (6) of Sec. III, depends on the parameter 0^+. In principle this parameter should be as small as possible, but in practice it cannot be too small because of the finite number of states used for the calculation. We represent in Fig. 13 the relative error on the density of states $n_0(E)$ of the empty lattice as a function of 0^+. This relative error is actually obtained by integrating the differences between the $n_0(E)$ of the computation and the analytical result $n_0(E)=\frac{2m}{h}\frac{ML}{\sqrt{2mE}}$, which serves as a reference. The results show that there is an optimal value for 0^+, which actually depends on the number of states $\Psi^{n,k}$ used for the calculation. If we refer to by E_{min} and E_{max} to the limits of the energies considered for the calculation of $n_0(E)$ and if n refers to the number of states whose energy $E^{n,k} \in [E_{\text{min}}, E_{\text{max}}]$, the optimal value of 0^+ is given approximately by

$$0^+_{\text{opt}} \sim 4.5\frac{E_{\text{max}} - E_{\text{min}}}{n}. \tag{A2}$$

The points predicted by this formula are represented in Fig. 13. For other applications, the factor 4.5 may have to be adapted depending on the context.

In Fig. 14, we represented the relative error on $n_0(E)$ as a function of M for different values of the cutoff energy. The parameter 0^+ is evaluated systematically using Eq. (A2), so that is independent of the particular value of E_{cutoff} ($E_{\text{cutoff}} > E_{\text{max}}$). The results show that $n_0(E)$ does not depend critically on E_{cutoff}, as long as E_{cutoff} is at least 2 eV larger than E_{max}. The relative error of $n_0(E)$ decreases as M increases, because of the higher density of points at which the band structure is calculated. The decrease of the relative error is inversely proportional to M, until a saturation at $\epsilon_{\text{bands}}/(E_{\text{max}}-E_{\text{min}})$ finally occurs. This is well illustrated by the result obtained using $N=40$ and $E_{\text{cutoff}}=20$ eV. The relative error at saturation is indeed of the order of 10^{-2} eV/10 eV$=10^{-3}$. Considering $N=80$ reduces ϵ_{bands} by a factor 4, which results in a reduction of the saturation level in Fig. 14 by this same factor. For the current application, $n_0(E)$ is already calculated with a relative accuracy of 10^{-3} using $M=8000$. Considering $M=20\,000$ results in an accuracy of the order of 5×10^{-4} (saturation level).

The influence of E_{cutoff} is better illustrated by looking at the accuracy of the bound states of Fig. 3(b), which is the

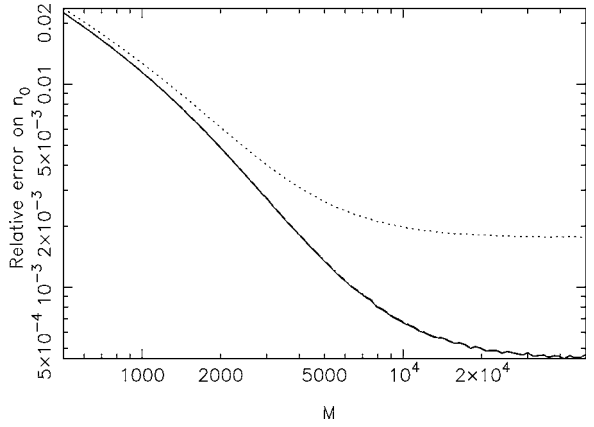

FIG. 14. Relative error on the density of states $n_0(E)$ of Fig. 3(a) (empty lattice), as a function of M. These results are calculated using $N=80$ and $E_{\text{cutoff}}=20$ eV (solid line), 30 eV (dashed line), and 40 eV (dot-dashed line). The dotted result is obtained using $N=40$ and $E_{\text{cutoff}}=20$ eV. The parameter 0^+ is evaluated according to Eq. (A2) and does not depend on the particular value of E_{cutoff}.

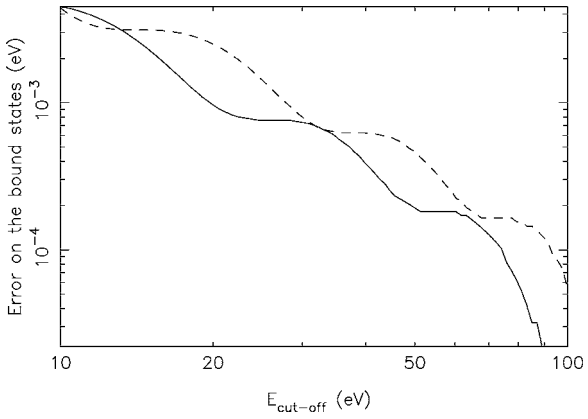

FIG. 15. Error on the first (solid line) and second (dashed line) bound states of Fig. 3(b) (empty lattice), as a function of E_{cutoff}. These results are calculated using $N=80$ and $M=8000$. The parameter 0^+ is evaluated according to Eq. (A2) and does not depend on the particular value of E_{cutoff}.

result presented in Fig. 15. These states are obtained after application of the techniques of Sec. III. Following the conclusions reached so far, we used $N=80$ and $M=8000$. The parameter 0^+ was evaluated again using Eq. (A2) (it is independent of E_{cutoff}). The results show that considering $E_{\text{cutoff}}=30$ eV enables one to reach an accuracy of 0.001 eV in the position of the two bound states. In order to get an accuracy of 10^{-4} eV, it is necessary to take $E_{\text{cutoff}}=95$ eV. It was checked that increasing M did not improve the accuracy (given the value of N and M is indeed close its saturation level). A good choice of parameters, in order to get results with a typical accuracy of 0.001 eV, is therefore to take $N=80$, $M=8000$, $E_{\text{cutoff}}=30$ eV, and 0^+ as given by Eq. (A2).

APPENDIX B: DERIVATION OF THE GREEN'S FUNCTION OF A ONE-DIMENSIONAL SYSTEM AT AN EIGENSTATE ENERGY

We demonstrate here the expression given in Eq. (5) for the Green's function of a one-dimensional system. This relation applies only to situations where the energy E considered is that of an eigenstate of the system ($E=E^{n,k}$). We drop for the moment the subscript j from the notation so that the positions are given by $x=i\Delta x$. We refer by Ψ^+ and Ψ^- to the two solutions of Schrödinger's equation at the energy $E^{n,k}$, which correspond to either a right-propagating state (+ sign) or a left-propagating state (− sign).

The canonical equation $[E^{n,k}-H^0]G^0=1$ relevant to the Green's function can be written explicitly like

$$(E^{n,k}-V_i^0)G_{i,i'}+\frac{\hbar^2}{2m}\frac{G_{i-1,i'}-2G_{i,i'}+G_{i+1,i'}}{\Delta x^2}=\delta_{i,i'}, \tag{B1}$$

and we postulate a solution of the form

$$G^0_{i,i'}(E^{n,k})=A\begin{cases}\Psi_i^-\Psi_{i'}^+ & \text{when } i\leqslant i',\\ \Psi_{i'}^-\Psi_i^+ & \text{when } i>i'.\end{cases} \tag{B2}$$

For $i>i'$, $(A\Psi_{i'}^-)\Psi_i^+$ is a valid solution of Eq. (B1) since $\delta_{i,i'}=0$ and Ψ_i^+ is a solution of Schrödinger's equation. It has the appropriate physical character of a right-going solution. For $i<i'$, $(A\Psi_{i'}^+)\Psi_i^-$ is also a valid solution of Eq. (B1), since again $\delta_{i,i'}=0$ and Ψ_i^- refers to a solution of Schrödinger's equation. It has the appropriate character of a left-going solution. Finally, when $i=i'$, Eq. (B1) is turned into

$$A\left[(E^{n,k}-V_i^0)\Psi_i^-\Psi_i^+ + \frac{\hbar^2}{2m\Delta x^2}(\Psi_{i-1}^-\Psi_i^+ - 2\Psi_i^-\Psi_i^+ + \Psi_i^-\Psi_{i+1}^+)\right] = 1. \tag{B3}$$

Using the fact that Ψ^+ and Ψ^- are solutions of Schrödinger's equation, one can replace $(E^{n,k}-V_i^0)\Psi_i^-\Psi_i^+$ by $-\frac{\hbar^2}{4m\Delta x^2}[(\Psi_{i-1}^+ - 2\Psi_i^+ + \Psi_{i+1}^+)\Psi_i^- + (\Psi_{i-1}^- - 2\Psi_i^- + \Psi_{i+1}^-)\Psi_i^+]$, so that the previous equation is finally turned into an expression that enables one to express A as

$$A=\frac{4m\Delta x^2}{\hbar^2}[\Psi_i^-(\Psi_{i+1}^+-\Psi_{i-1}^+)-\Psi_i^+(\Psi_{i+1}^--\Psi_{i-1}^-)]^{-1}. \tag{B4}$$

The quantity $W=\Psi_i^-(\Psi_{i+1}^+-\Psi_{i-1}^+)-\Psi_i^+(\Psi_{i+1}^--\Psi_{i-1}^-)$ is the numerical equivalent of the Wronskien. This quantity turns out to be constant, so that the particular value of i used to evaluate W is of a reduced significance. The fact W is constant is demonstrated by writing $\Delta W/\Delta x$ as

$$\frac{\Delta W}{\Delta x}=\Psi_i^-\frac{\Psi_{i+1}^+-2\Psi_i^++\Psi_{i-1}^+}{\Delta x}-\Psi_i^+\frac{\Psi_{i+1}^--2\Psi_i^-+\Psi_{i-1}^-}{\Delta x}$$
$$=\Psi_i^-\frac{2m\Delta x}{\hbar^2}(V_i^0-E^{n,k})\Psi_i^+-\Psi_i^+\frac{2m\Delta x}{\hbar^2}(V_i^0-E^{n,k})\Psi_i^-=0, \tag{B5}$$

where we have used again the fact Ψ^+ and Ψ^- are solutions of Schrödinger's equation. Numerically, for the applications presented in this paper, the ratio between the standard deviation of W and its average on the N points of an elementary cell reaches a maximum of the order of 10^{-12}. When considering the whole set of states for which W is evaluated, the relative deviation is around 10^{-15} on average. The amplitude of these deviations does not depend sensitively on the parameters of our technique.

The demonstration of Eq. (5) is finally achieved by identifying Ψ_i^+ with $\Psi_{i,j}^{n,k}$ and Ψ_i^- with $(\Psi_{i,j}^{n,k})^*$. This last substitution is only valid for a real-valued potential energy, while the results expressed in this appendix in terms of Ψ^+ and Ψ^- would also apply to complex-valued potentials.

[1] J. Callaway, *Quantum Theory of the Solid State*, student ed. (Academic Press, New York, 1976), p 398.
[2] E. N. Economou, *Green's Functions in Quantum Physics* (Springer, Berlin, 1983).
[3] M. Mardaani and K. Esfarjani, Chem. Phys. **317**, 43 (2005).
[4] C. Buth, U. Birkenheuer, M. Albrecht, and P. Fulde, Phys. Rev. B **72**, 195107 (2005).
[5] I. V. Zozoulenko, F. A. Maao, and E. H. Hauge, Phys. Rev. B **53**, 7975 (1996).
[6] P. A. Knipp and T. L. Reinecke, Phys. Rev. B **54**, 1880 (1996).
[7] G. R. C. Tai and R. P. Shaw, J. Acoust. Soc. Am. **56**, 796 (1974).
[8] T. Chen-To, *Dyadic Green Functions in Electromagnetic Theory* (IEEE Press, New York, 1993).
[9] A. Dereux, J.-P. Vigneron, Ph. Lambin, and A. A. Lucas, Phys. Rev. B **38**, 5438 (1988).
[10] A. I. Rahachou and I. V. Zozoulenko, Phys. Rev. B **72**, 155117 (2005).
[11] K. K. Yee, IEEE Trans. Antennas Propag. **14**, 302 (1966).
[12] A. Taflove, *Computational Electrodynamics: The Finite-Difference Time-Domain Method* (Artech House, Reading, MA, 1995).
[13] M. Krumpholz and L. P. B. Katehi, IEEE Trans. Antennas Propag. **44**, 555 (1996).
[14] J. M. Johnson and Y. Rahmat-Samii, Microwave Opt. Technol. Lett. **14**, 101 (1997).
[15] J. Vazquez and C. G. Parini, Electron. Lett. **35**, 554 (1999); **35**, 1033 (1999).
[16] W. L. Ma, M. R. Rayner, and C. G. Parini, IEEE Trans. Antennas Propag. **53**, 339 (2005).
[17] R. de L. Kronig and W. G. Penney, Proc. R. Soc. London, Ser. A **130**, 499 (1931).
[18] C. Kittel, *Physique de l'Etat Solide*, 7th ed. (Dunod, Paris, 1998).
[19] B. V. Numerov, Publ. Observ. Central Astrophysic. Russ. **2**, 188 (1933).
[20] H. Q. Nguyen, P. H. Cutler, T. E. Feuchtwang, N. Miskovsky, and A. A. Lucas, Surf. Sci. **160**, 331 (1985).
[21] J.-P. Vigneron and Ph. Lambin, J. Phys. A **13**, 1135 (1980).
[22] G. Lenz and J. Salzman, Appl. Phys. Lett. **56**, 871 (1990).
[23] D. Indjin, V. Milanovic, and Z. Ikonic, Phys. Rev. B **52**, 16762 (1995).
[24] A. Kaczynski, R. Kucharczyk, and M. Steslicka, Physica E (Amsterdam) **13**, 59 (2002).
[25] W.-Q. Huang, K.-Q. Chen, Z. Shuai, L. Wang, W. Hu, and B. S. Zuo, Physica E (Amsterdam) **28**, 374 (2005).
[26] I. Tamm, Phys. Z. Sowjetunion **1**, 733 (1932).
[27] W. Shockley, Phys. Rev. **56**, 317 (1939).
[28] H. Ohno, E. E. Mendez, J. A. Brum, J.-M. Hong, F. Agullo-Rueda, L. L. Chang, and L. Esaki, Phys. Rev. Lett. **64**, 2555 (1990).
[29] F. Y. Huang, Appl. Phys. Lett. **57**, 1669 (1990).
[30] W. L. Bloss, Phys. Rev. B **44**, 8035 (1991).
[31] R. Kucharczyk, M. Steslicka, A. Akjouj, B. Djafari-Rouhani, L. Dobrzynski, and E. H. El Boudouti, Phys. Rev. B **58**, 4589 (1998).
[32] W.-Q. Huang, K.-Q. Chen, Z. Shuai, L. Wang, and W. Hu, Phys. Lett. A **325**, 70 (2004).
[33] J. M. Ziman, *Principles of the Theory of Solids* (Cambridge University Press, Cambridge, England, 1964) pp. 46–48.
[34] M. Bescond, J. L. Autran, D. Munteanu, and M. Lannoo, Solid-State Electron. **48**, 567 (2004).
[35] D. Straub and F. J. Himpsel, Phys. Rev. B **33**, 2256 (1986).
[36] B. E. Granger, P. Kral, H. R. Sadeghpour, and M. Shapiro, Phys. Rev. Lett. **89**, 135506 (2002).